Picosecond nonlinearity of GeO_2–Bi_2O_3–PbO–TiO_2 glasses at 532 and 1,064 nm

**Valentin Besse · Alexandre Fortin · Georges Boudebs ·
Paula S. Valle · Marcelo Nalin · Cid B. de Araújo**

Abstract The third-order optical properties of GeO_2–Bi_2O_3–PbO–TiO_2 glasses at 532 nm and 1,064 nm were studied to evaluate their potential for optical limiting and all-optical switching. The Z-scan technique was used to determine the nonlinear (NL) refractive index, n_2, and the NL absorption coefficient, α_2, of samples with different amounts of the constituent oxides. Values of $n_2 \approx +0.7 \times 10^{-14}$ cm^2/W at 1,064 nm and $\approx +1.5 \times 10^{-14}$ cm^2/W at 532 nm were measured. The NL absorption coefficient, α_2, was smaller than the minimum that our apparatus can measure ($\alpha_2 < 0.01$ cm/GW) in the near-infrared (1,064 nm); in the visible region (532 nm), we obtained $\alpha_2 \approx 4.4$ cm/GW. The set of NL parameters measured indicates the potential usefulness of the GeO_2–Bi_2O_3–PbO–TiO_2 glasses for all-optical switching at 1,064 nm and for optical limiting at 532 nm.

1 Introduction

Nonlinear (NL) optical studies of heavy-metal oxide (HMO) glasses were first reported about two decades ago [1, 2] and have been attracting much attention because of their large nonlinearity and fast response time. From the basic point of view, studies of HMO glasses were performed to characterize their behavior as hosts for luminescent ions, the NL propagation of light pulses, NL refraction, and NL absorption, among other phenomena [3–5]. From the applied point of view, there is large interest in HMO glasses for applications in all-optical switching (AOS), optical limiting (OL), lasers, optical amplification, and NL optical fibers [4, 6–10]. In particular, the third-order susceptibility, $\chi^{(3)}$, of various glasses containing at least one of the following compounds Bi_2O_3, PbO, TeO_2, WO_3, and TiO_2, has been investigated under different excitation conditions. It is recognized that the high NL response of HMO glasses is mainly due to the large hyperpolarizability of the constituent compounds that are highly influenced by lone-electron pairs in the cations, and by non-bridging oxygen bonds [4]. The third-order nonlinearity of some promising oxide glasses for NL photonics such as Bi_2O_3–B_2O_3–TiO_2 [11], Bi_2O_3–GeO_2–TiO_2 [12], Bi_2O_3–ZnO–B_2O_3 [13], $NaPO_3$–WO_3–Bi_2O_3 [14, 15], $Pb(PO_3)_2$–WO_3 [16], $NaPO_3$–BaF_2–WO_3 [17], Bi_2O_3–WO_3–TeO_2 [18], and PbO–Ga_2O_3–Bi_2O_3 [19] was investigated. At 800 nm (100 fs regime), the figure-of-merit, $FOM = n_2/\alpha_2\lambda$ (where λ is the laser wavelength, $n_2 \propto Re\chi^{(3)}$ and $\alpha_2 \propto Im\chi^{(3)}$) for the glasses in [12, 15] was larger than 1. At 1,064 nm (17 ps and 80 ps regime), the glasses $Pb(PO_3)_2$–WO_3, PbO–Ga_2O_3–Bi_2O_3, and $NaPO_3$–WO_3–Bi_2O_3 present $FOM \approx 1$ and the glass Bi_2O_3–ZnO–B_2O_3 presents $FOM \approx 4$. More recently, the glass TeO_2–GeO_2–K_2O–Bi_2O_3 [20] was developed, and it was measured FOM = 3.3 at 800 nm and FOM = 2.35 at 1,064 nm.

In this paper, we report NL measurements of GeO_2–Bi_2O_3–PbO–TiO_2 glasses with various compositions that have better characteristics than it was recently presented in

V. Besse · A. Fortin · G. Boudebs · C. B. de Araújo
LPhiA, Laboratoire de Photoniques d'Angers, LUNAM
Université, Université d'Angers, EA 4464,
49045 Angers Cedex 01, France

P. S. Valle · M. Nalin
LAVIE - Instituto de Química, Universidade do Estado de São
Paulo – UNESP, C.P. 676, Araraquara, SP 14800-060, Brazil

C. B. de Araújo (✉)
Departamento de Física, Universidade Federal de Pernambuco,
Recife, PE 50670-901, Brazil
e-mail: cid@df.ufpe.br

[20]. The new glasses, with PbO and TiO_2 replacing K_2O and TeO_2 in the glass TeO_2–GeO_2–K_2O–Bi_2O_3, were fabricated to exploit the larger polarizability of Pb looking for a composition more suitable for AOS at 1,064 nm and OL at 532 nm. Films of GeO_2–Bi_2O_3–PbO–TiO_2 glass were previously used to fabricate two-dimensional photonic crystals [21], but its optical NL response was not studied before. In Sect. 2, we describe the synthesis method used for production of the samples and give details of the measurement techniques used. In Sect. 3, we describe the NL technique used to characterize the samples and discuss the results obtained in comparison with previously studied materials. Finally, in Sect. 4, we present a summary of the work.

2 Experimental details

Glass samples with compositions $(100–x)[0.45GeO_2$–$0.33Bi_2O_3$–$0.22PbO]$–$xTiO_2$ (with x = 0, 5, 10, and 20, in mol %) were prepared using the melting–quenching method. Germanium oxide (Alfa Aesar Puratronic 99.999 pure), bismuth oxide (Aldrich 99.9 pure), lead oxide (Synth 98.0 pure), and titanium oxide (Aldrich 99.9 pure) were mixed in a mortar before transfer to a platinum crucible. The chemical batches were put into an electric furnace and left to melt during 1 h at 1,200 °C. After homogenization and fining, the temperature of the furnace was decreased to 1,100 °C before to cast the liquid into a stainless steel mold, pre-heated at 350 °C. The glasses were left at such temperature during 2 h for annealing in order to decrease the internal stress of the samples due to the quenching process. Latter, the furnace was turned off and left to reach the room temperature under its natural cooling rate. The glass transition temperature, T_g, and the onset of crystallization, T_x, were determined by differential scanning calorimetry (DSC). Thin glass pieces were set in platinum pans under N_2 atmosphere and heated at 10 °C/min. The estimated error for both T_g and T_x is ± 2 °C: The glass pieces were optically polished using conventional sand papers with different granulometries. The samples studied were labeled as follows: sample A—x = 0; sample B—x = 5; sample C—x = 10; and sample D—x = 20.

The optical absorption spectra were measured using a commercial spectrophotometer, and the refractive indices were obtained by the prism coupling technique. The refractive indices results can be expressed with high precision, but we considered only two significant digits that are sufficient to determine the NL parameters.

For the NL experiments, it was used a mode-locked Nd:YAG laser (Coherent, 1,064 nm; 17 ps; 10 Hz) and its second harmonic at 532 nm. The measurements were performed using the Z-scan technique [22] that allows measurements of n_2 and α_2.

3 Results and discussion

Figure 1 shows the absorbance spectra of the samples that present large transparency window from the green to the near-infrared. The linear absorption coefficient measured was $\alpha_0 < 3$ cm^{-1} for the two laser wavelengths used. The samples present optical bandgap at ≈ 450 nm. The values of T_g and T_x are presented in Table 1 as well as the thermal stability parameter $\Delta T = T_x - T_g$.

Figure 2 shows a scheme of the setup used for the NL measurements. The Z-scan setup is integrated in a 4f-system composed of two convergent lenses with equal focal lengths (20 cm). The output image of the 4f-system is acquired in a 1,000 × 1,018 pixels cooled CCD camera operated at −30 °C with fixed gain. The sample is scanned
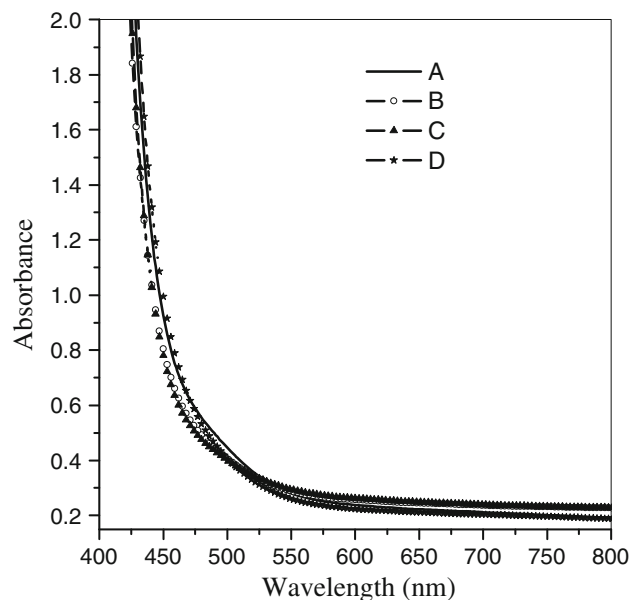

Fig. 1 Absorbance spectrum. Samples thicknesses: A 1.4; B 1.1; C 1.1; D 1.8 mm

Table 1 TiO_2 samples' composition, characteristic temperatures (T_g for glass transition; T_x for the onset of crystallization), and thermal stability parameter $\Delta T = T_x - T_g$

| Sample	TiO_2 composition (mol %)	T_g (°C)	T_x (°C)	ΔT (°C)
A	0	385	470	85
B	5	402	489	87
C	10	425	524	99
D	20	459	567	108
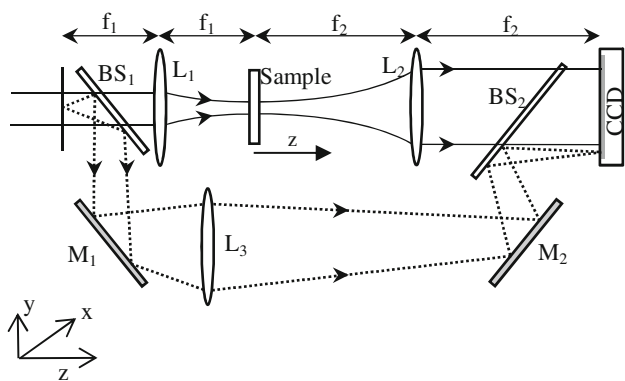
Fig. 2 Schematic of the 4f-system for the Z-scan measurements ($f_1 = f_2$). The sample d is scanned in the focal region along the beam propagation direction. The *labels* refer to lenses (L$_1$–L$_3$); mirrors (M$_1$, M$_2$); beam splitters (BS$_1$, BS$_2$)
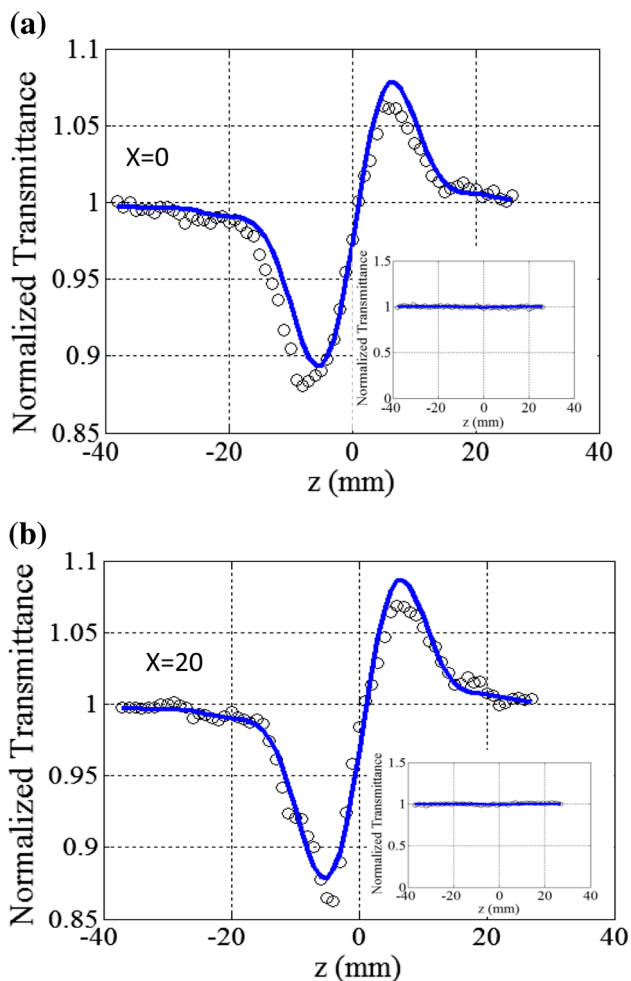
Fig. 3 *Closed-aperture* Z-scan profiles at 1,064 nm **a** sample A ($x = 0$); **b** sample D ($x = 20$). The *insets* show the corresponding *open-aperture* profiles
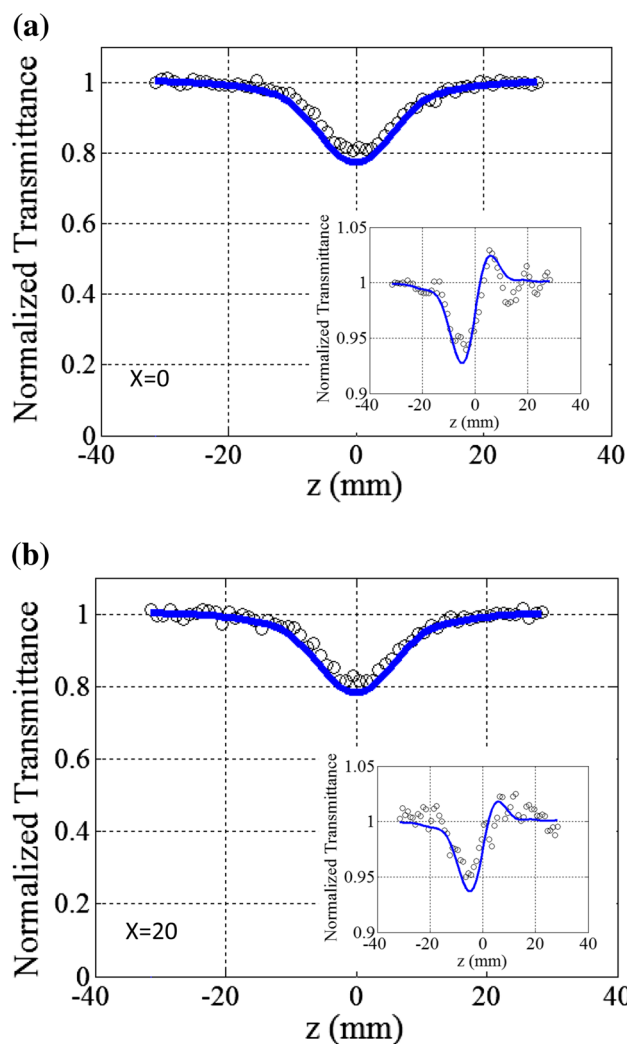
Fig. 4 Open-aperture Z-scan profiles at 532 nm **a** sample A ($x = 0$); **b** sample D ($x = 20$). The *insets* show the *closed-aperture* profiles

in the focal region along the beam propagation direction (Z axis). *Open-* and *closed-aperture* Z-scan transmittances were numerically processed from the acquired images by integrating over all pixels in the first case and over a circular numerical filter in the *closed-aperture* case, corresponding to a linear aperture transmittance S = 0.73 to optimize the sensitivity and the signal-to-noise ratio [23, 24]. The incident intensity was adjusted by a polarizer–waveplate system at the entry of the Z-scan setup. The laser intensity inside the samples was 7.0 GW/cm^2 (0.9 GW/cm^2) at 1,064 nm (532 nm), and the calibration was based on the NL refractive index of CS$_2$ given in Ref. [22].

Figure 3 shows results for the samples A and D. The *closed-aperture* Z-scan profiles at 1,064 nm indicated self-focusing nonlinearity, and the insets, corresponding to the

Table 2 Linear and nonlinear parameters of the samples: n_0 is the linear refractive index, n_2 is the nonlinear refractive index, and α_2 is the nonlinear absorption coefficient

Sample	n_0 1,064/ 543 nm	1,064 nm		532 nm	
		n_2 (10^{-14} cm^2/ W)	α_2 (cm/ GW)	n_2 (10^{-14} cm^2/W)	α_2 (cm/GW)
A	2.2/2.3	0.70 ± 0.14	<0.01	1.9 ± 0.5	4.4 ± 0.4
B	2.2/2.3	0.70 ± 0.15	<0.01	1.4 ± 0.4	4.4 ± 0.4
C	2.2/2.3	0.64 ± 0.12	<0.01	1.3 ± 0.3	4.3 ± 0.5
D	2.2/2.3	0.80 ± 0.16	<0.01	1.6 ± 0.5	4.3 ± 0.5

open-aperture Z-scan profiles, show negligible NL absorption. The other samples present similar behavior. Figure 4 shows the results for excitation at 532 nm. Self-focusing nonlinearity is also observed in this case for all samples; however, large NL absorption is detected. Because the NL absorption is more important in the 532 nm case, we present the *closed-aperture* Z-scan profile as insets of Fig. 4.

The solid lines in Figs. 3 and 4 are drawn using parameters given in Table 2 (for details of the calculation procedure see [23, 24]). Notice that the n_2 values did not change much with the samples' compositions. NL absorption was not observed in the *open-aperture* Z-scan experiments at 1,064 nm indicating that α_2 is smaller than the minimum we can detect (0.01 cm/GW). In the experiments at 532 nm, it was observed large NL absorption as illustrated in Fig. 4a, b that shows *open-aperture* Z-scan profiles corresponding to $\alpha_2 \approx 4.4$ cm/GW.

The values of n_2 at 1,064 nm are ≈ 30 times larger than for silica [25] and 10 times larger than for TeO$_2$–GeO$_2$–K$_2$O–Bi$_2$O$_3$ [20] measured under the same conditions. The α_2 values (4.4 cm/GW) measured at 532 nm are comparable with the values reported for typical semiconductors under degenerate two-photon excitation [26, 27]. n_2 and α_2 are not expected to change much in the samples studied because the TiO$_2$ hyperpolarizability has the same order of magnitude than the glass constituents that are substituted due to the TiO$_2$ addition.

In the 532 nm experiments, the samples presented photo-induced effects (PIE) when large intensities were used, but the results reported here were obtained for 0.9 GW/cm^2 in order to prevent the influence of PIE. As reported in [28], the Z-scan apparatus used allows identification of PIE by performing another Z-scan measurement in the linear regime (lower laser intensity) after the NL measurement.

Using the data of Table 2, we may compare the results obtained in this work and the previous results of [20].

Considering that the values of $\alpha_2 < 0.01$ cm/GW, we see that the present glass composition shows an improvement in the figure-of-merit for all-optical switching, FOM $= n_2/\alpha_2\lambda$, due to the larger n_2 values obtained. The values of *FOM* for the present samples vary from 6 to 7.5 which are 250 % larger than in [20]. Notice that the FOM was calculated considering $\alpha_2 = 0.01$ cm/GW, but the actual *FOM* can be even larger because α_2 can be much smaller. Of course, the good result in the infrared is due to the simultaneous presence of the heavy cations Bi^{3+}, Pb^{2+}, and Ti^{4+} that contribute for the larger NL refraction.

The results obtained in the 532 nm experiments are also better than the ones obtained for NaPO$_3$–BaF$_2$–WO$_3$ glasses [17] that present n_2 values ≈ 70 % smaller and α_2 values ≈ 10 times smaller than for the present glass composition. The value of $\alpha_2 \approx 4.4$ cm/GW reported here indicates that the GeO$_2$–Bi$_2$O$_3$—PbO–TiO$_2$ glass compositions are appropriate for optical limiting at 532 nm in the picosecond regime.

Notice also from Table 1 that the glass compositions studied present values of the thermal stability parameter $\Delta T = T_x - T_g$ comparable to the other glasses already used to fabricate microstructured optical fibers [8, 9, 27] being a good candidate for integrated photonics in the visible and near-infrared. In particular notice that the thermal stability parameters of the glasses studied here are larger than the ones in Ref. [20].

4 Summary

The 1,064 nm experiments herein reported provide values for the third-order susceptibility of new HMO glass compositions that present large NL refractive indices and small NL absorption. This indicates an improvement in the figure-of-merit for picosecond all-optical switching that in the present case corresponds to $n_2/\lambda\alpha_2 > 6$ at 1,064 nm. On the other hand, the values of the NL absorption coefficient at 532 nm are comparable or even larger than other HMO compositions previously studied. The present results indicate the large potential of GeO$_2$–Bi$_2$O$_3$–PbO–TiO$_2$ glasses for optical limiting in the visible range.

References

1. J. Yumoto, S.G. Lee, B. Kippelen, N. Peyghambarian, B.G. Aitken, N.F. Borrelli, Appl. Phys. Lett. **63**, 2630 (1993)
2. S. Smolorz, I. Kang, F. Wise, B.G. Aitken, N. F. Borrelli, J. Non-Cryst. Solids **256/257**, 310 (1999)
3. R.L. Sutherland, *Handbook of Nonlinear Optics* (Wiley, New York, 1996)
4. M. Yamane, Y. Asahara, *Glasses for Photonics* (Cambridge University Press, Cambridge, 2000)
5. F. Träger (ed.) *Springer Handbook of Lasers and Optics.* (Springer Science, New York, 2007)
6. R.A.H. El-Mallawany, *Tellurite Glasses Handbook: Physical Properties and Data,* 2nd ed. (CRC Press, Boca Raton, 2012)
7. J. Ren, G. Dong, S. Xu, R. Bao, J. Qiu, J. Phys. Chem. A **112**, 3036 (2008)
8. D. Manzani, Y. Ledemi, I. Skripachev, Y. Messaddeq, S.J.L. Ribeiro, R.E.P. de Oliveira, C.J.S. de Matos, Opt. Mater. Express **1**, 1515 (2011)
9. D. Manzani, J.L. Ferrari, F.C. Polachini, Y. Messaddeq, S.J.L. Ribeiro, J. Mater. Chem. **22**, 16540 (2012)
10. S. Maning, H. Ebendorff-Heidepriem, T.M. Monro, Opt. Mater. Express **2**, 140 (2012)
11. X. Tiefeng, C. Feifei, D. Shixum, N. Qiuhua, S. Xiang, W. Xunsi, Phys. B **404**, 2012 (2009)
12. F. Chen, B. Song, C. Lin, S. Dai, J. Cheng, J. Heo, Mater. Chem. Phys. **135**, 73 (2012)
13. A.S.L. Gomes, E.L. Falcão-Filho, C.B. de Araújo, D. Rativa, R.E. de Araujo, K. Sakaguchi, F.P. Mezzapesa, I.C.S. Carvalho, P.G. Kazansky, J. Appl. Phys. **101**, 033115 (2007)
14. D. Manzani, C.B. de Araújo, G. Boudebs, Y. Messaddeq, S.J.L. Ribeiro, J. Phys. Chem. B **117**, 408 (2013)
15. F.E.P. dos Santos, C.B. de Araújo, A.S.L. Gomes, K. Fedus, G. Boudebs, D. Manzani, Y. Messaddeq, J. Appl. Phys. **106**, 063507 (2009)
16. T.R. Oliveira, K. Fedus, D. Manzani, E.L. Falcão-Filho, G. Boudebs, C.B. de Araújo, Y. Messaddeq, J. Appl. Phys. **108**, 103523 (2010)
17. E.L. Falcão-Filho, C.B. de Araújo, C.A.C. Bosco, L.H. Acioli, G. Poirier, Y. Messaddeq, G. Boudebs, M. Poulain, J. Appl. Phys. **96**, 2525 (2004)
18. Y. Chen, Q. Nie, T. Xu, S. Daí, X. Wang, X. Shen, J. Non-Cryst, Solids **354**, 3468 (2008)
19. C.B. de Araújo, E.L. Falcão-Filho, A. Humeau, D. Guichaoua, G. Boudebs, L.R.P. Kassab, Appl. Phys. Lett. **87**, 221904 (2005)
20. T.A. Oliveira, D. Manzani, E.L. Falcão-Filho, Y. Messaddeq, G. Boudebs, K. Fedus, C.B. de Araújo, Appl. Phys. B Rapid Commun. (to be published). doi:10.1007/s00340-014-5835-9
21. L.F. Avila, J.M.P. Almeida, M.S. Gonçalves, P.S. Valle, M. Nalin, C.R. Mendonça, L. Cescato, in *Published in SPIE Proceedings—vol. 8776. Holography: advances and modern trends III*, ed. by M. Hrabovský, J.T. Sheridan, A. Fimia-Gil (2013). doi: 10.1117/12.2018734
22. M. Sheik-Bahae, A.A. Said, T.H. Wei, D.J. Hagan, E.W. van Stryland, IEEE J. Quantum Electron. **QE-26**, 760 (1990)
23. K. Fedus, G. Boudebs, Opt. Commun. **292**, 140 (2013)
24. K. Fedus, G. Boudebs, Opt. Commun. **284**, 1057 (2011)
25. D. Milam, Appl. Opt. **37**, 546 (1998)
26. C.M. Cirlogane, L.A. Padilha, D.A. Fishman, S. Webster, D.J. Hagan, E.W. van Stryland, Opt. Express **19**, 22951 (2011)
27. X. Feng, A.K. Mairaj, D.W. Hewak, T.M. Monre, J. Lightwave Technol. **23**, 2046 (2005)
28. G. Boudebs, C.B. de Araujo, Appl. Phys. Lett. **85**, 3740 (2004)